Helical Superstructures

DOI: 10.1002/anie.201410975

# Design of Aromatic Helical Polymers for STM Visualization: Imaging of Single and Double Helices with a Pattern of π–π Stacking**

*Junyan Zhu, Zeyuan Dong,* Shengbin Lei, Lili Cao, Bing Yang, Wenfang Li, Yuanchao Zhang, Junqiu Liu,* and Jiacong Shen*

**Abstract:** *From scanning tunneling microscopy (STM) images of rationally designed helical polymers with a pattern of π–π stacking, we successfully identified the single- and double-helical superstructures. The STM images of the helical structures revealed the smallest helical architecture (diameter ca. 1.3 nm) that has been seen so far. Furthermore, the interconversion of single and double helices was further underpinned by experimental analyses. Significantly, the formation of double helices induced different supramolecular chirality to that observed for the single helices.*

As the principal structural components of biopolymers, helices have attracted much attention owing to their importance in molecular recognition, molecular programming, and catalysis. Inspired by Nature, chemists have established the growing research area of foldamer chemistry to mimic the structures and functions of biopolymers and to explore their potential application in sensors, enantiomer separation, asymmetric catalysis, and materials science.[1,2] In helical structures, the strong tendency toward helical folding is attributed to various driving forces in the form of both intramolecular and intermolecular interactions, including electrostatic, solvophobic, π–π, hydrogen-bonding, and van der Waals interactions. The structural diversity and ample availability of driving forces provide an ideal platform for the rational design of enormous covalent and noncovalent helical structures with aromatic,[2–5] aliphatic,[6] and even hybrid backbones.[7]

Artificial helical structures can be identified by conventional structure-characterization methods, including crystallography[3,8] and various spectrographic techniques. Notably, corroboration of the conformation of helical polymers has mainly relied on circular dichroism (CD) spectroscopy. Recently, significant progress has been made in the characterization of molecular structures by single-molecule imaging techniques. In particular, atomic force microscopy (AFM) has been widely used to elucidate molecular structures with sensitivities approaching those required for the identification of single molecules and atoms.[9] In pioneering studies on the characterization of helical polymers by AFM imaging, Yashima and co-workers clearly represented the outside molecular morphology of helical polymers,[10,11] such as poly(*meta*-phenylene ethynylene)s, with the current highest resolution of about 1.03 nm.[5] AFM characterization is clearly restricted to the observation of the inside pattern of helical polymers.[11–13] Therefore, scanning tunneling microscopy (STM) is an important tool to complement single-molecule imaging techniques.[12,14]

Herein, we describe the design of a new type of aromatic helical architecture consisting of the repeating structural motif 2,5-bis(2-pyridyl)-1,3,4-oxadiazole for STM imaging. Three conformations described as cisoid I, cisoid II, and transoid (see Figure S1 in the Supporting Information) seem to be plausible in the structural motif. Conformational analysis demonstrated that the cisoid I conformation is the most stable of the three. The difference in Gibbs free energy between the cisoid I and cisoid II conformations is remarkable ($\Delta G = 20.96\ \mathrm{kJ\,mol^{-1}}$, Figure 1a), thus indicating that electrostatic repulsion in the structural motif plays an essential role in stabilizing the cisoid I conformation. The crystal structure of 2,5-bis(2-pyridyl)-1,3,4-oxadiazole also undoubtedly proved that the structural motif adopts the cisoid I conformation.[15] Repeated sequences of this structural motif with the cisoid I conformation should give rise to a helical architecture (Figure 1b,c, see below).

The helical polymer **1** (Figure 2a) was prepared by a straightforward synthetic procedure and fully characterized (see Figure S2 and comments in the Supporting Information).[16] The molecular weight of polymer **1** was confirmed by MALDI-TOF MS to have a value of up to 12000, which indicated that the degree of polymerization can be up to 30 (see Figure S5). The number-average molecular weight ($M_n$) and polydispersity index (PDI) of polymer **1** were estimated to be $6.0 \times 10^3$ and 1.16, respectively.

CD measurements were carried out to prove the helical conformation of polymer **1** in solution. The racemic helical polymer **1** did not show any CD signal (Figure 2b). When (*S*)-1-phenylethanamine and (*R*)-1-phenylethanamine were covalently introduced at the termini of polymer **1**, CD spectra gave rise to opposite signals at 370 nm (Figure 2b), which clearly demonstrated the formation of a right-handed and a left-handed helix, respectively.[17]

[*] Dr. J. Y. Zhu, Prof. Z. Y. Dong, Prof. B. Yang, Dr. W. F. Li, Y. C. Zhang, Prof. J. Q. Liu, Prof. J. C. Shen
State Key Laboratory of Supramolecular Structure and Materials
College of Chemistry, Jilin University
2699 Qianjin Street, Changchun 130012 (P.R. China)
E-mail: zdong@jlu.edu.cn
junqiuliu@jlu.edu.cn
Prof. S. B. Lei, Dr. L. L. Cao
Key Laboratory of Micro-systems and Micro-structures Manufacturing, Ministry of Education, Harbin Institute of Technology
2 Yikuang Street, Nan Gang District, Harbin 150080 (P.R. China)

[**] This research was supported by the National Natural Science Foundation of China (No. 21274051, 21234004, 21420102007, 21221063).

Supporting information for this article is available on the WWW under http://dx.doi.org/10.1002/anie.201410975.

  

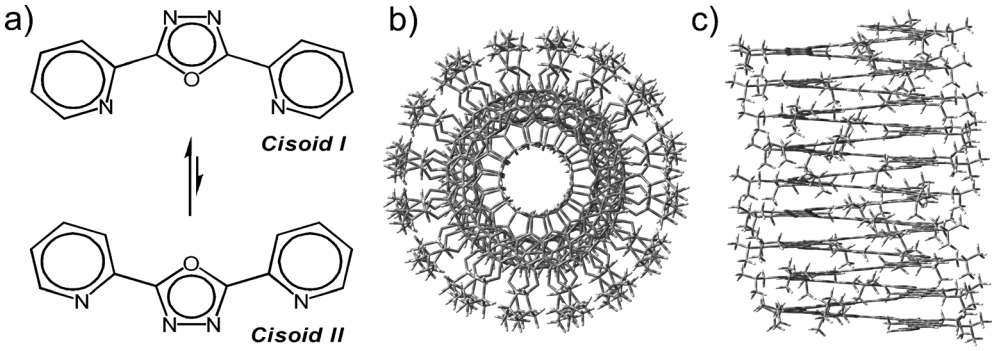


***Figure 1.*** a) Cisoid I and cisoid II conformations of the structural motif 2,5-bis(2-pyridyl)-1,3,4-oxadiazole: The geometries were optimized at the DFT/B3LYP/6-31g(d,p) level. b) Top view and c) side view of the most stable conformation of the designed polymeric model with 30 repeating units, as calculated with the COMPASS force field.

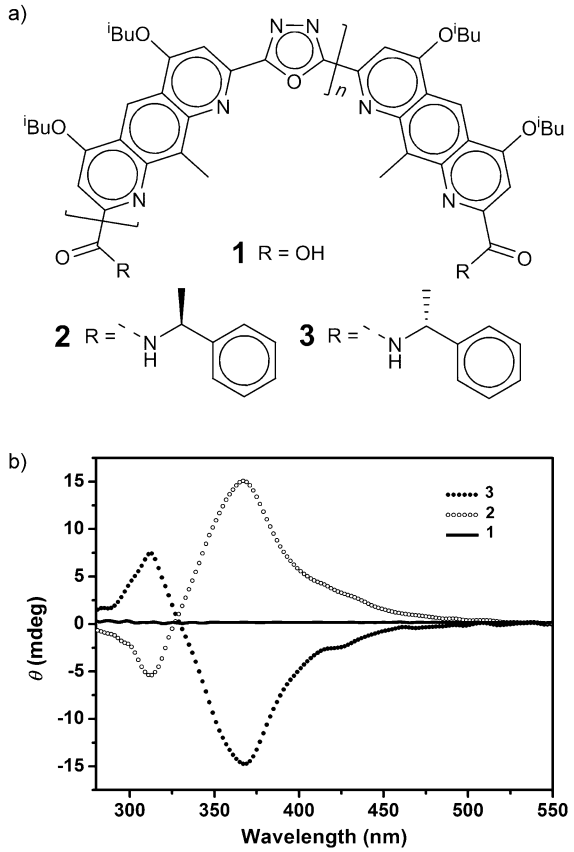


***Figure 2.*** a) Molecular structures of helical polymers **1**, **2**, and **3**. b) CD spectra of polymers **1**, **2**, and **3** at the same concentration of 0.23 g L$^{-1}$ in dichloromethane at room temperature.

We used wide-angle X-ray powder diffraction (XRD) to obtain structural information about polymer **1**. Several structurally characteristic reflections (2.50, 1.18, 0.49, and 0.36 nm) in the XRD pattern (Figure 3a; see also Table S1 in the Supporting Information) provided detailed structural information about polymer **1** that related well to its helical structure (Figure 3b,c). The peak position at 2.50 nm most likely corresponds to the spacing distance between two proximal parallel helical polymers (Figure 3d). As expected, besides electrostatic repulsion, the occurrence of the peak position at 0.36 nm corresponding to the distance of a π–π interaction was evidence that polymer **1** forms a stable helical conformation with the assistance of intramolecular π–π interactions.

Considering the structural features in the repeated sequences of polymer **1**, we used a polymeric model with 30 repeating units to calculate the most stable conformation by two different types of force-field analysis on the basis of the XRD data (see Figure S7). Computational results indicated that the most stable conformation of the 30 mer had a helical shape with a diameter of (2.4 ± 0.1) nm, an inner backbone diameter of (1.4 ± 0.1) nm, a helical pitch of (0.39 ± 0.05) nm, and (3.2 ± 0.1) units per turn (Figure 1b,c). The vertical distance between two adjacent helical planes corresponding to the spacing distance of π–π interactions should be less than 0.39 nm (see Figure S13), in accordance with the XRD result (0.36 nm; Figure 3b). Molecular simulation supported the hypothesis that the peak positions at 1.18 and 0.49 nm in the XRD pattern correspond to the spatial distances between the side chains of the helical polymer **1** (Figure 3c), in analogy with a previous observation.[5]

STM is a powerful tool for the direct observation of helical structures of polymers. The STM images of polymer **1** deposited on a graphite surface demonstrated a well-organized self-assembled monolayer of straight and uniform helical columns packed in parallel to each other with a spacing distance of (2.3 ± 0.1) nm (Figure 4a–e), which is in good agreement with the result found by XRD (2.5 nm; Figure 3d). The width of the bright part of columns was measured to be (1.3 ± 0.1) nm, which is attributed to the aromatic backbone of polymer **1** with higher electron density, whereas the dark area between these columns corresponds to the side aliphatic groups. These periodic oblique stripes, clearly the result of a one-handed helical array, are addressed as either left-handed helices or right-handed helices (see Figure S8). A high-resolution STM image revealed single-stranded helices of polymer **1**, in which the helical pitch was measured to be (0.42 ± 0.09) nm (Figure 4b). Importantly, when the concentration of polymer **1** increased, the high-resolution STM images (Figure 4c,d), in which the emerging helical conformations showed a similar diameter and twofold larger helical pitch (mean value: (0.96 ± 0.09) nm) as compared to those of the single helices, revealed a double-stranded helix structure. This conclusion was supported by a previous crystallographic study[16,18] and also by different STM patterns (Figure 4). In the STM images, the calculated distances ((0.42 ± 0.09) nm; see Figures S9, S10, and S13) of intramolecular π–π interactions in single helices seem to be slightly bigger than those

  

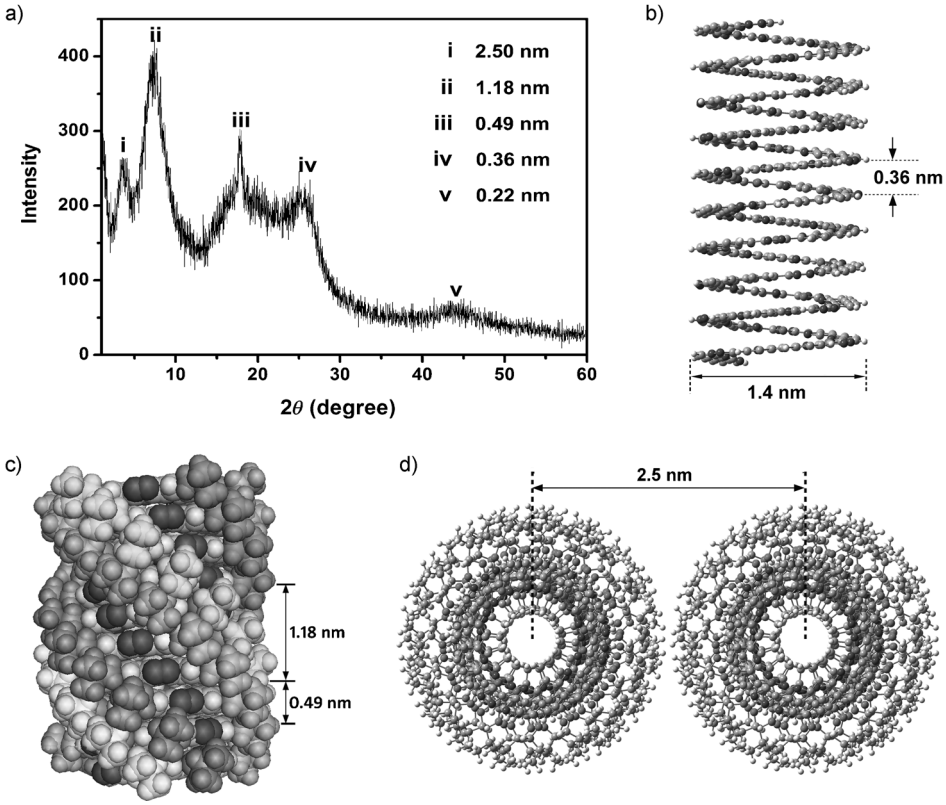


***Figure 3.*** a) XRD pattern of polymer **1**. The *d* spacing corresponding to each peak is listed. b) Inner aromatic helical backbone in the model 30 mer. The spacing distance of the π–π interaction is 0.36 nm. c) Arrangement of the side chains of the helical polymer, as represented by space-filling models. d) Spacing distance between two adjacent helical polymers.

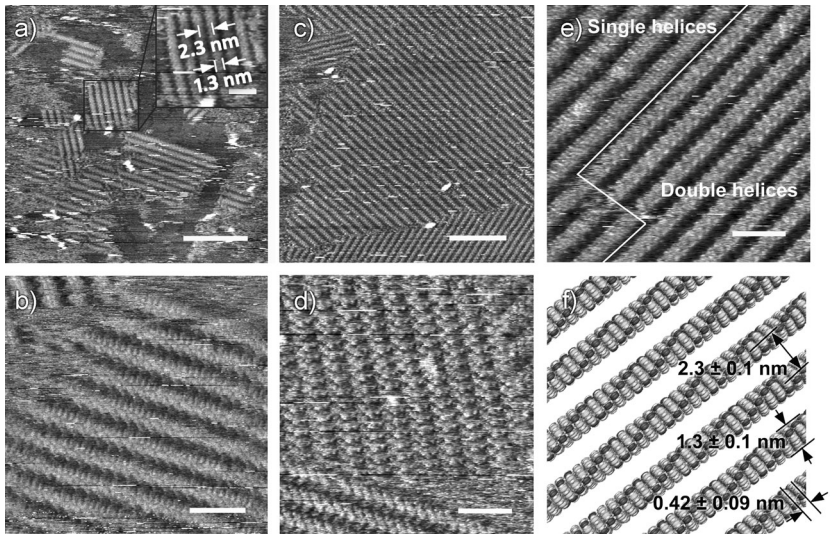


***Figure 4.*** a) STM image and partial enlarged view of polymer **1** (0.10 g L$^{-1}$); scale bars: 20 nm, 5 nm (inset). b) High-resolution STM image of **1** (0.10 g L$^{-1}$); scale bar: 5 nm. c) STM image of **1** (1.0 g L$^{-1}$); scale bar: 20 nm. d) High-resolution STM image of **1** (1.0 g L$^{-1}$); scale bar: 5 nm. e) High-resolution STM image: single helices (upper left) and double helices (lower right); scale bar: 5 nm. f) Schematic illustration of a regenerated arrangement of single-helical backbones with right-handedness.

found by XRD and molecular modeling. This result could be attributed to the existence of a possible different mode of the helices when adsorbed to the highly ordered pyrolytic graphite (HOPG) surface (see Figure S12). Significantly, the image in Figure 4e directly proved that the polymer **1** can self-assemble from single helices to double helices through dimerization driven by intermolecular π–π stacking interactions. Moreover, a transmission electron microscopy (TEM) image of polymer **1** (see Figure S16) is completely consistent with the STM measurements. Furthermore, owing to the self-assembly of **1**, supramolecular helical polymers of more than 100 nm in length were observed on the surface (Figure 4c). Dynamic light scattering (DLS) experiments also demonstrated the occurrence of supramolecular assemblies (see Figure S17).

We carried out UV/Vis titrations to monitor the interconversion of single and double helices.[3,16,18] As the amount of water increased, the absorbance gradually decreased at 250, 280, and 402 nm; however, the intensity at about 450 nm increased (Figure 5b). In accordance with a previous study,[16] this observation clearly indicated a transition from single helices **1** to double helices $(\mathbf{1})_2$. At the same time, a temperature-dependent UV/Vis titration (see Figure S18) revealed an opposite change corresponding to a transition from double helices $(\mathbf{1})_2$ to single helices **1** as the temperature increased. Fluorescence titrations also showed that this transition took place. As the concentration of polymer **1** increased, the fluorescence intensity increased almost linearly at first, and then decreased in steps at an excitation wavelength of 402 nm (see Figure S19). When the excitation wavelength was changed to 462 nm, a similar change was observed (Figure 5c). Remarkably, when the concentration of polymer **1** was increased, the maximum fluorescence emission wavelength changed from 529 to 549 nm, and then remained constant above a concentration of about 2.0 g L$^{-1}$ (Figure 5d). A bathochromic shift up to 20 nm implied a clear transition from single helices **1** to double helices $(\mathbf{1})_2$ involving intermolecular π–π aromatic interactions. According to the results of fluorescence titrations, the

  

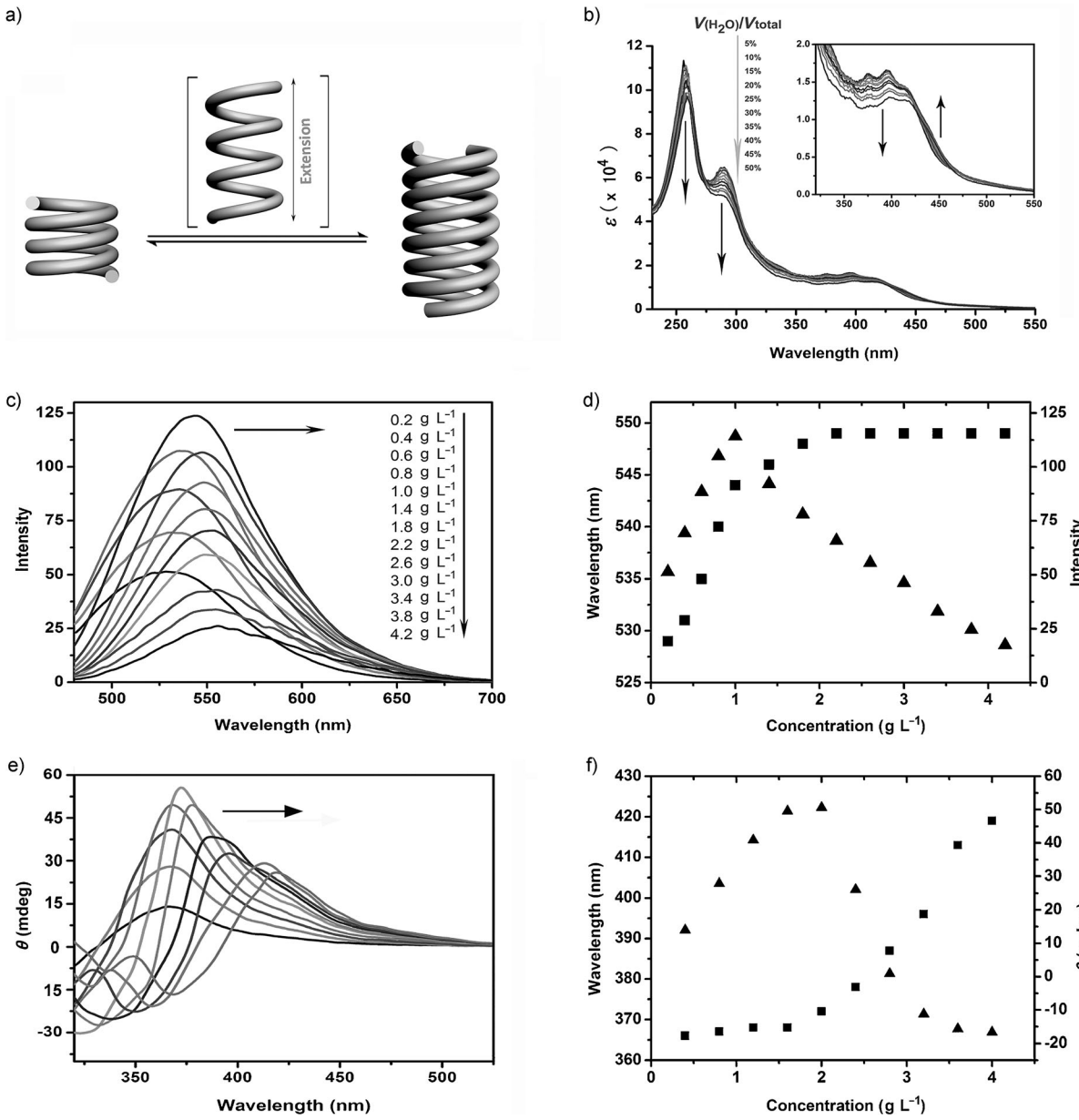


***Figure 5.*** a) Schematic representation of the interconversion between single and double helices. b) UV/Vis titration of polymer **1** in which the volume fraction of $H_2O$ in $CH_3CN$ was increased at 25 °C. c) Fluorescence titration of polymer **1** at different concentrations from 0.2 to 4.2 g L$^{-1}$ in pyridine at an excitation wavelength of 462 nm. d) Variation in the fluorescence intensity at 529 nm (triangles) and the wavelength of the maximum fluorescence emission (squares) versus the concentration of polymer **1** in pyridine at 25 °C. e) CD spectra of polymer **2** at various concentrations from 0.4 to 4.0 g L$^{-1}$ in pyridine at 25 °C. f) Variation in the CD intensity at 370 nm (triangles) and in the CD maximum wavelength (squares) of **2** versus its concentration in pyridine at 25 °C.

dimerization constant ($K_{dim}$) was calculated to be above $5.0 \times 10^4$ L mol$^{-1}$ at 25 °C in pyridine (see Figure S20). Temperature-dependent NMR spectroscopic experiments with polymer **1** provided further evidence of the interconversion between single and double helices. When the temperature was increased to 80 °C, new signals corresponding to single helices appeared (see Figure S21) owing to the dissociation of double-stranded helices.

To further underpin the interconversion between single and double helices, we carried out concentration-dependent CD titrations in pyridine (Figure 5e). When the concentration of the right-handed polymer **2** was increased from 0.4 to 1.6 g L$^{-1}$, the CD intensity at 370 nm increased almost linearly (Figure 5f). When the concentration of **2** was increased further beyond 2.0 g L$^{-1}$, a turning point emerged, and the CD intensity at 370 nm decreased significantly. Moreover, a remarkable intensity decrease (see Figure S22) at the maximum absorption wavelength and a large bathochromic shift in the CD spectrum (Figure 5f) both illustrated the process of single helices converting into double helices through the dimerization of helical polymers by intermolecular π–π aromatic interactions as the concentration changed.

  

In conclusion, we have designed and prepared a type of aromatic helical polymer for STM imaging. Strikingly, we observed the STM images of single and double helices at the single-molecule level. The STM images clearly showed helical architectures in which the distance between the turns was defined by π–π interactions. Furthermore, the interconversion between single and double helices was clearly corroborated by various spectrographic characterization techniques. The formation of double helices from single helices gave rise to a remarkable change in the supramolecular chirality. Moreover, self-assembly of helical polymers into well-ordered supramolecular assemblies was clearly visualized on the surface. The synthetically accessible system will be available for the development of nanometer-scale single molecules that might be applicable in controllable self-assembly as well as potential functional materials.

Received: November 18, 2014
Revised: December 19, 2014
Published online: February 4, 2015

**Keywords:** aromatic polymers · dimerization · helical structures · π interactions · scanning tunneling microscopy

[1] a) S. H. Gellman, *Acc. Chem. Res.* **1998**, *31*, 173 – 180; b) D. J. Hill, M. J. Mio, R. B. Prince, T. S. Hughes, J. S. Moore, *Chem. Rev.* **2001**, *101*, 3893 – 4011; c) E. R. Gillies, F. Deiss, C. Staedel, J. M. Schmitter, I. Huc, *Angew. Chem. Int. Ed.* **2007**, *46*, 4081 – 4084; *Angew. Chem.* **2007**, *119*, 4159 – 4162; d) *Foldamers: Structure, Properties, and Applications* (Eds.: S. Hecht, I. Huc), Wiley-VCH, Weinheim, **2007**; e) E. Yashima, K. Maeda, H. Iida, Y. Furusho, K. Nagai, *Chem. Rev.* **2009**, *109*, 6102 – 6211.

[2] a) D. W. Zhang, X. Zhao, J. L. Hou, Z. T. Li, *Chem. Rev.* **2012**, *112*, 5271 – 5316; b) D. Haldar, H. Jiang, J. M. Leger, I. Huc, *Angew. Chem. Int. Ed.* **2006**, *45*, 5483 – 5486; *Angew. Chem.* **2006**, *118*, 5609 – 5612.

[3] V. Berl, I. Huc, R. G. Khoury, M. J. Krische, J. M. Lehn, *Nature* **2000**, *407*, 720 – 723.

[4] a) K. Oh, K. S. Jeong, J. S. Moore, *Nature* **2001**, *414*, 889 – 893; b) B. Gong, H. Q. Zeng, J. Zhu, L. H. Yua, Y. H. Han, S. Z. Cheng, M. Furukawa, R. D. Parra, A. Y. Kovalevsky, J. L. Mills, E. Skrzypczak-Jankun, S. Martinovic, R. D. Smith, C. Zheng, T. Szyperski, X. C. Zeng, *Proc. Natl. Acad. Sci. USA* **2002**, *99*, 11583 – 11588; c) R. M. Meudtner, S. Hecht, *Angew. Chem. Int. Ed.* **2008**, *47*, 4926 – 4930; *Angew. Chem.* **2008**, *120*, 5004 – 5008.

[5] M. Banno, T. Yamaguchi, K. Nagai, C. Kaiser, S. Hecht, E. Yashima, *J. Am. Chem. Soc.* **2012**, *134*, 8718 – 8728.

[6] a) M. M. Müller, M. A. Windsor, W. C. Pomerantz, S. H. Gellman, D. Hilvert, *Angew. Chem. Int. Ed.* **2009**, *48*, 922 – 925; *Angew. Chem.* **2009**, *121*, 940 – 943; b) I. M. Mándity, E. Weber, T. A. Martinek, G. Olajos, G. K. Toth, E. Vass, F. Fulop, *Angew. Chem. Int. Ed.* **2009**, *48*, 2171 – 2175; *Angew. Chem.* **2009**, *121*, 2205 – 2209; c) L. Guo, A. M. Almeida, W. C. Zhang, A. G. Reidenbach, S. H. Choi, I. A. Guzei, S. H. Gellman, *J. Am. Chem. Soc.* **2010**, *132*, 7868 – 7869.

[7] a) J. H. K. K. Hirschberg, L. Brunsveld, A. Ramzi, J. A. J. M. Vekemans, R. P. Sijbesma, E. W. Meijer, *Nature* **2000**, *407*, 167 – 170; b) M. Kudo, V. Maurizot, B. Kauffmann, A. Tanatani, I. Huc, *J. Am. Chem. Soc.* **2013**, *135*, 9628 – 9631.

[8] Q. Gan, Y. Ferrand, C. Y. Bao, B. Kauffmann, A. Grelard, H. Jiang, I. Huc, *Science* **2011**, *331*, 1172 – 1175.

[9] a) J. Welker, F. J. Giessibl, *Science* **2012**, *336*, 446 – 449; b) J. Zhang, P. C. Chen, B. K. Yuan, W. Ji, Z. H. Cheng, X. H. Qiu, *Science* **2013**, *342*, 611 – 614.

[10] T. Nishimura, K. Takatani, S. Sakurai, K. Maeda, E. Yashima, *Angew. Chem. Int. Ed.* **2002**, *41*, 3602 – 3604; *Angew. Chem.* **2002**, *114*, 3754 – 3756.

[11] a) J. Kumaki, S. i. Sakurai, E. Yashima, *Chem. Soc. Rev.* **2009**, *38*, 737 – 746; b) E. Yashima, K. Maeda, Y. Furusho, *Acc. Chem. Res.* **2008**, *41*, 1166 – 1180; c) S. S. Sheiko, M. Möller, *Chem. Rev.* **2001**, *101*, 4099 – 4123.

[12] K. Shinohara, S. Yasuda, G. Kato, M. Fujita, H. Shigekawa, *J. Am. Chem. Soc.* **2001**, *123*, 3619 – 3620.

[13] P. Samorí, H. Engelkamp, P. A. de Witte, J. A. E. Rowan, R. J. M. Nolte, J. P. Rabe, *Adv. Mater.* **2005**, *17*, 1265 – 1268.

[14] A. Cricenti, S. Selci, A. C. Felici, R. Generosi, E. Gori, W. Djaczenko, G. Chiarotti, *Science* **1989**, *245*, 1226 – 1227.

[15] F. Emmerling, I. Orgzall, G. Reck, B. W. Schulz, S. Stockhause, B. Schulz, *J. Mol. Struct.* **2006**, *800*, 74 – 84.

[16] E. Berni, B. Kauffmann, C. Y. Bao, J. Lefeuvre, D. M. Bassani, I. Huc, *Chem. Eur. J.* **2007**, *13*, 8463 – 8469.

[17] a) A. Tanatani, A. Yokoyama, I. Azumaya, Y. Takakura, C. Mitsui, M. Shiro, M. Uchiyama, A. Muranaka, N. Kobayashi, T. Yokozawa, *J. Am. Chem. Soc.* **2005**, *127*, 8553 – 8561; b) C. Dolain, H. Jiang, J. M. Leger, P. Guionneau, I. Huc, *J. Am. Chem. Soc.* **2005**, *127*, 12943 – 12951.

[18] a) M. L. Singleton, G. Pirotte, B. Kauffmann, Y. Ferrand, I. Huc, *Angew. Chem. Int. Ed.* **2014**, *53*, 13140 – 13144; *Angew. Chem.* **2014**, *126*, 13356 – 13360; b) H. Goto, Y. Furusho, E. Yashima, *J. Am. Chem. Soc.* **2007**, *129*, 109 – 112.

  